

# Dual-context Identification based on Geometric Descriptors for 3D Registration Algorithm Selection

Polycarpo Souza Neto<sup>a</sup>, José Marques Soares<sup>b</sup>, Michela Mulas<sup>c</sup>  
and George André Pereira Thé<sup>d</sup>

*Department of Teleinformatics Engineering, Federal University of Ceara, Fortaleza CEP 60455-970, Brazil*

**Keywords:** Point Cloud Registration, Iterative Closest Point, Generalized ICP, Eigentropy, Omnivariance.

**Abstract:** In 3D reconstruction applications, matching between corresponding point clouds is commonly resolved using variants of the Iterative Closest Point (ICP). However, ICP and its variants suffer from some limitations, functioning properly only for some contexts with well-behaved data distribution; outdoor scene, for example, poses many challenges. Indeed, the literature has suggested that the ability of some of these algorithms to find a match was reduced by the presence of geometric disorder in the scene, for example. This article presents a method based on the characterization of the eigentropy and omnivariance properties of clouds to indicate which variant of the ICP is best suited for each context considered here, namely, object or outdoor scene alignment. In addition to the context selector, we suggest a partitioning step prior to alignment, which in most cases allows for reduced computational cost. In summary, the proposal as a whole worked satisfactorily to the alignment as a multipurpose registration technique, serving to pose correction of data from different contexts and thus being useful for computer vision and robotics applications.

## 1 INTRODUCTION


In three-dimensional image processing, the problem of point cloud registration associated to small objects as well as to wide outdoor environments has been intensively studied in the last few decades for its importance in a wide range of applications, including human recognition (Siqueira et al., 2018), agriculture (Chebrolu et al., 2018) and autonomous driving (Levinson et al., 2011). These two categories of scenarios differ in many aspects, including the 3D image size, the susceptibility to cluttering, the influence of surface deformations among sequential shots, etc, what poses different challenges to algorithms dealing with one or other category. Indeed, in the literature there has always been an effort to associate the scene context and the registration technique that best suits the given scenario. For example, objects have been dealt with from Iterative Closest Point-based registration algorithms. Especially, ICP point-to-point implementation has been reported in many contribu-


tions (Besl and McKay, 1992). Although it is a pioneer technique, limitations regarding the computational efforts have led to many variants; one of such is the approach presented in (Souza Neto et al., 2018), in which registration is performed on sub-cloud space after a cloud partitioning of the original data. As an iterative technique, ICP is susceptible to falling into local minima, and the literature has provided important advances in that matter, as it is the generalized algorithm named GICP (Segal et al., 2009). In view of that association between registration technique and the context regarding the scenario, we have posed the problem of automatic identifying them as a prior step to the registration itself. The contribution brought in this paper is not on the selection only, but it is one that comprises the use of the registration algorithm as the alignment core in a point-cloud partitioning approach.


## 2 RELATED WORKS


### 2.1 Point Cloud Registration

Since the introduction of the ICP algorithm (Besl and McKay, 1992), a number of variants have been pro-

<sup>a</sup>  <https://orcid.org/0000-0001-5057-1942>

<sup>b</sup>  <https://orcid.org/0000-0002-5111-5794>

<sup>c</sup>  <https://orcid.org/0000-0001-9120-2465>

<sup>d</sup>  <https://orcid.org/0000-0002-8064-8901>

posed in the literature to overcome its limitations. For example, random (Zhang, 1994) or uniform down-sampling (Vitter, 1984). Although the classical sampling strategies may be very useful for computational reasons when dense clouds are concerned, for sparse point clouds they might lead to loss of relevant information instead. An efficient approach to registration 3D data from outdoor scenes is demonstrated in (Segal et al., 2009). It explores planar patches in both point clouds, which takes to plan to plan concept.

For real-world applications involving 3D scene perception, time-performance is a must, and naturally a look at recent applications is worth. In (Forte et al., 2021), authors solved a problem related to UAV-pose estimation from a point-cloud registration assisted estimation algorithm relying on the linear version of Kalman Filter. In that case, the solution achieved 10% correction in volume estimation of a large coal stockpile in a thermal power plant. To be stressed that the registration algorithm relied on a cloud-partitioning approach (Souza Neto et al., 2018) with GICP (Segal et al., 2009) as alignment core.

Despite the fact that all those techniques provided self-consistent and comprehensible description of the manipulations and transformations done in the point clouds during the registration itself, it is to be mentioned the proposition of deep learning approaches in the field. In that domain, it is worth mentioning the recent contribution in (Kurobe et al., 2020), which introduces Corsnet, a solution working on the basis of many intermediate convolutional layers of local and global data retrieved directly from the 3D image samples. Since point clouds are particularly dense data in its essence, and deep learning methods represent a completely different paradigm regarding data representation, in the present work no additional attention is paid to that, though we recognize its relevance and the recent rise of interest of the scientific community.

## 2.2 Eigen-features

Important works in the literature of 3D image processing report on spatial representation of surfaces from a geometric description point of view. In many of them, parameters calculated from the eigenvalues of the covariance matrix associated to the point cloud are used as features for classification or recognition purposes. For example, in (Hackel et al., 2016), authors were able to perform efficient countour detection in 3D outdoor scenario.

Other important papers are (Demantké et al., 2011) and (Donoso et al., 2017). In [(Demantké et al., 2011), authors introduced a vicinity-based approach for lines, surface and sphere detection from entropy-

like measurements of the point clouds. In (Donoso et al., 2017), eigentropy is revisited and seems to apply well to the points selection problem, but details on the normalization of the entropy associated measures are missed or neglected in the discussion.

We highlight that those papers are mostly interested in segmentation; furthermore, in the bibliographic search done so far, we have found no papers suggesting to use entropy or covariance matrix-derived parameters as descriptors for scene context identification. This appear as a gap in literature, which we intend to cover for in the present contribution.

## 3 MATHEMATICAL FORMULATION

The technique here proposed is a registration algorithm with dual-context selection alternative. It is a cloud-partitioning approach in the sense that input data are segmented into smaller groups of points. Figure 1 illustrates that. Sections in the following provide details on the sub-cloud grouping, on the choice of partitioning direction and on the dual-context selection procedure for the alignment core.

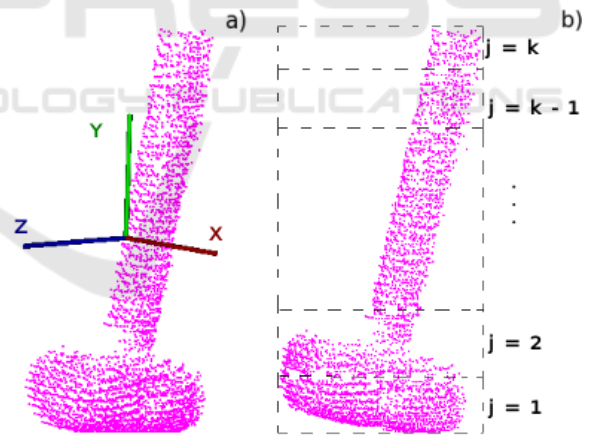


Figure 1: In (a), we have the Hammer model and the representation of the respective directions, while in (b), we have an analogy to partitioning, where  $j$  is the index for each partition.

### 3.1 Cloud Partitioning Approach

Let  $(S)$  and  $(T)$  be the source and target models to undergo registration; partitioning is here defined as the grouping operation of the whole point sets into smaller groups, or sub-clouds, which are here indexed by  $j$ , with  $j = 1$  to  $k$  groups. It starts with a ordering procedure similar to *quicksort* implementation

along a given  $\xi$ -axis, which can be one of the principal  $\hat{x}, \hat{y}, \hat{z}$ -axes. Details on the axis choice for partitioning is given in the next section. The vectors  $Q\vec{s}_i$  e  $Q\vec{t}_m$  represent the points lying within source and target models after the ordering. They sub-clouds can then be defined according to the following sets:

$$S_j = \left\{ Q\vec{s}_i \mid (j-1) \cdot \frac{N_S}{k} < i < j \cdot \frac{N_S}{k} \right\} \quad (1)$$

$$T_j = \left\{ Q\vec{t}_m \mid (j-1) \cdot \frac{N_T}{k} < m < j \cdot \frac{N_T}{k} \right\} \quad (2)$$

in which  $N_S$  e  $N_T$  are the size of source and target models, respectively. The reader should note that, from the formation law of the above equations above show that the grouping is nothing else than a collection of points taken contiguously in lots of  $\frac{N_T}{k}$  or  $\frac{N_S}{k}$  points.

### 3.2 Choice of Partitioning Axis

In the current version of the partitioning approach, the choice regarding the axis along t which the grouping is done relies on the spatial distribution of points. It starts with the calculation of the centroid coordinates of the points and an offset in the whole points set, making them zero-mean centered:

$$\mu = \frac{1}{N} \sum_{i=1}^N \vec{x}_i. \quad (3)$$

$$\vec{x}_k = \vec{x}_i - \mu, \forall i, k \in [1, N] \quad (4)$$

The covariance matrix can then be calculated

$$\Sigma_X = \frac{1}{N} \sum_{i=1}^N \vec{x}_i \vec{x}_i^T \quad (5)$$

and its eigenvalues can be put in order

$$\lambda_3 \leq \lambda_2 \leq \lambda_1 \quad (6)$$

where  $\lambda_1$ , the largest one, is chosen as the partitioning axis.

### 3.3 Alignment Core Selection Criterion

Besides being useful for the partitioning-axis choice, the data spatial distribution information as measured by the eigenvalues and eigenvectors of the covariance matrix can be used to calculate descriptors for the point clouds. In the present work, we investigated the sum of eigenvalues, omnivariance, eigentropy, linearity, planarity, sphericity, anisotropy and surface change for a large dataset of objects and outdoor

scenes. In that preliminary study, the goal was to see which of those descriptors could lead to acceptable inter-class discrimination between object and outdoor scene contexts. The analysis counted on 2D plots of those characteristics, for a total of 64 pairwise combinations. The dataset had 100 samples equally distributed into the two classes. Table I synthetizes that.

During the analysis, we got results as those shown in Figure 2, and two particular descriptors revealed as promising measurements for good discrimination in the dual-context identification, namely the eigentropy and the omnivariance. For the other pairwise combinations (even those not shown here for brevity), significant overlap in the 2D space were observed. The robustness of those two descriptors may be explained by the fact that they are less susceptible to data size and density, making them suitable for situations in which intraclass discrimination is not a goal.

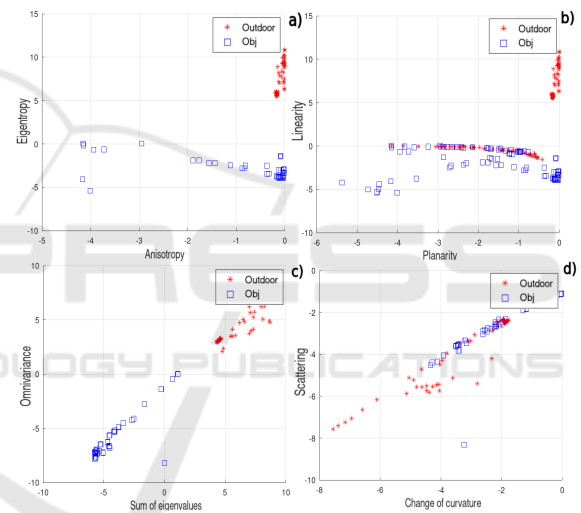


Figure 2: Pairwise dispersion diagram of geometric descriptors for the datasets of each context. In (a) we have the anisotropy plot  $\times$  eigentropy, in (b) flatness  $\times$  linearity, in (c) sum of eigenvalues  $\times$  omnivariance and in (d) scattering  $\times$  change of curvature.

In the present work, the geometric descriptors named eigentropy and omnivariance are calculated directly from the covariance matrix eigenvalues, with no additional normalization on them, according to:

$$E_\lambda = - \sum_{i=1}^3 \lambda_i \log(\lambda_i); \quad (7)$$

$$O_\lambda = \prod_{i=1}^3 (\lambda_i)^{1/3}. \quad (8)$$

For what concerns the preliminary study reported in Figure 1, the calculated geometric descriptors were collected for a large set of samples of objects and

Table 1: Division of data used in the regression process.

Class	Dataset	Instances
Objects	Stanford (Levoy et al., 2005) (36 samples)	Bunny: Rotations: 0 to 315 degree; Buddha and Dragon: 0 to 336 degrees; Armadillo: 0 to 270 degrees.
	Parma (Aleotti et al., 2014) (14 samples)	Horse: 0 and 180 degrees; Hammer: 0 and 45 degrees; Fustino grande: 0 to 270 degrees; Fustino piccolo: 0 to 315 degrees.
Scenes	Bremen (Wulf, 2016) (13 samples)	–
	Hannover (Oliveira and Tavares, 2014) (10 samples)	–
	Priority dataset (27 samples)	Department (Two samples); Camp (Fifteen samples); Stockpile (Ten samples);

outdoor, as well. For both measurements, when they are taken independently, a threshold of nearly  $\simeq 0.4619$  provided good separation line between the two classes investigated. Following the reasoning given in (Donoso et al., 2017), we associate low values of entropy-based measurements to well-behaved points distribution like in solid and compact objects (less disorder), whereas higher entropy suggests increased disorder and, as such, points to uncontrolled outdoor environments. This leads to the very simple decision rule for a given input point cloud model:

$$\begin{aligned} \text{if } \log(E_{\lambda}^S, O_{\lambda}^S) \leq 0.4619, \text{ core} = \text{ICP}_{pp} \\ \text{otherwise, core} = \text{GICP}. \end{aligned} \quad (9)$$

Once the context is identified, (if object or outdoor scene), then the registration itself is triggered. Whenever an object is identified, the point-to-point version of the ICP algorithm adapted to the cloud-partitioning framework discussed so far is used. One of the main differences of this adaptation regards the cost function of the ICP registration, which is now in sub-cloud space calculated as:

$$E_j(\Psi)_{ICP} = \frac{k}{N} \sum_{i=1}^{\frac{N}{k}} \|M_j - \Psi S_j\|, \quad (10)$$

where the index  $j$  refers to partitions undergoing registration in a given iterative step,  $N$  is the cloud size and index  $i$  refers to a given point lying on the partition  $j$ . In the equation,  $\Psi$  gives the rigid transformation relating input source and target models, which is the expected outcome of a registration algorithm. On the other hand, if an outdoor scene is identified, GICP algorithm adapted to the cloud-partitioning framework discussed so far is used. Compared to the traditional version (Segal et al., 2009), the adaptation regards the cost function equation of the GICP algo-

rithm, which now in sub-cloud space calculated resembles like:

$$E_j(\Psi)_{GICP} = \frac{k}{N} \sum_{i=1}^{\frac{N}{k}} d_i^{(\Psi)^T} (\Sigma_i^{M_j} + \Psi \Sigma_i^{S_j} \Psi^T)^{-1} d_k^{(\Psi)}, \quad (11)$$

where  $d_i^{(\Psi)^T}$  gives the point-to-point distance in the correspondence step, and  $\Sigma_i^{S_j}$  and  $\Sigma_i^{M_j}$  give the covariances for the vicinity of points in the  $j$ -th subclouds of source and target models. The whole registration approach proposed in the present work is summarized in the flowchart of Figure 3.

## 4 RESULTS

In this section, we discuss results for different registration experiments through a comparative analysis among algorithms. They include Go-ICP (Yang et al., 2016), CP-ICP (Souza Neto et al., 2018), CP-GICP (Forte et al., 2021), ICP variants (Besl and McKay, 1992) (Chen and Medioni, 1992) (Segal et al., 2009), the one named 3D-NDT (Magnusson et al., 2007), also the 4PCS (Aiger et al., 2008) and, finally, the algorithm SAC IA+ICP (Liu et al., 2020). For what concerns the 3D models, the dataset of objects includes samples from (Levoy et al., 2005) and from (Aleotti et al., 2014). The samples of outdoor scenes are the ones from (Wulf, 2016) and also some shots acquired after aerial imaging at an university campus (Forte et al., 2021). The whole set of algorithms were C++ written in the PCL framework (Rusu and Cousins, 2011), except for the Go-ICP whose executable was made available and run on a 12 GB Intel Core i5-8265U.

For additional information regarding the simulations (code implementation and parameters),

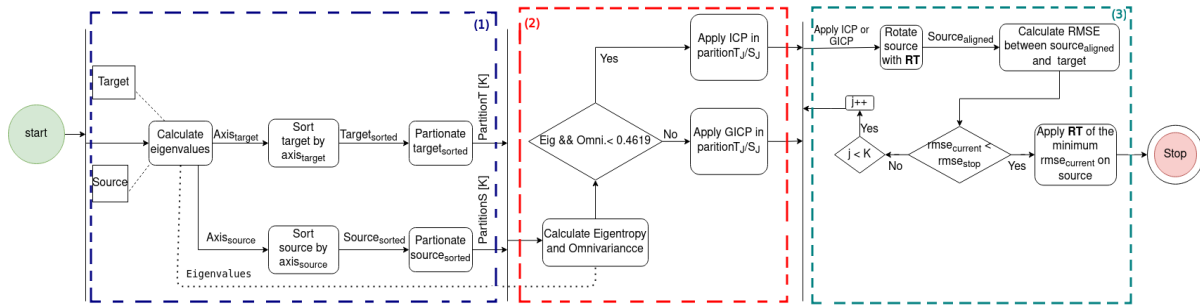


Figure 3: Flowchart of the proposed method. We have, respectively, in (1) the partitioning step, in (2) the choice of the alignment algorithm and in (3) the verification of the registration.

the reader is suggested to check the material available at <https://github.com/pneto29/>. For visualization of every result discussed in this paper, refer to <https://drive.google.com/drive/folders/1Mt5tavDks5LPtBNFumdW6rhgaSXE5fxO?usp=sharing>.

#### 4.1 Heatmap of Geometric Descriptors

Initially, we report on the use of the geometric descriptors and their ability to get the scene context. Figure 4 represent the pairwise similarity of Eigentropy and Omnivariance measurements as a heatmap, thus allowing for a simple perception of how good they are to distinguish between objects and outdoor scenario classes. We see how those two measurements are good at preserving intraclass similarity whilst separating well interclass sample pairs. For better comprehension of the above mentioned, in the color bar at right, the separation line between objects and outdoor scenes are shown for each geometric descriptor assessed.

#### 4.2 Pairwise Registration of Objects

We report here on the pairwise registration of objects; it can be thought of as a validation experiment, since the ground-truth (GT) is available. For quantitative assessment of matching goodness, Table 2 brings the root-mean square error between source and target models after registration. To help comparing the methods, Tables 3 and Tables 4 report the achieved pose correction (along with the ground-truth) and the time spent by each algorithm during registration.

Globally, we see that, although our technique is not the fastest in every case, it reaches a very good trend when analyzed under the presence of matching goodness requirement. In other words, ours can be lazier when Dragon model are subject to matching, but it is very good at doing the matching in both qualitative (see Figures 5(a) to 5(d)) and quantitative as-

essment (see Tables 2 and 3).

It is worth mentioning some words about 4PCS algorithm. Although it is a feature-space algorithm, and thus conceptually different to points-coordinate space approaches as ICP variants, its close efficiency and good time performance achieved in some of the investigated cases would suggest that it deserves some attention, perhaps in the context of a future investigation of a cloud-partitioning approach with 4PCS feature representation embedded in the sub-cloud space.

Table 2: RMSE obtained from registration between pairs of objects.

(*10 <sup>-3</sup> )	Bunny	Dragon	Happy Buddha	Hammer
<i>ICP<sub>p2p</sub></i>	<b>2.026</b>	<b>1.835</b>	<b>2.537</b>	<b>3.535</b>
4PCS	2.664	2.311	2.791	9.001
SAC IA	2.823	2.205	3.123	3.544
Go-ICP	89.000	55.000	32.000	207.000
CP-ICP	11.985	1.886	2.565	4.017
Our	<b>2.222</b>	<b>1.886</b>	<b>2.621</b>	<b>3.807</b>

Table 3: Rotation obtained from the registration of pairs of objects. Note the first row of the table, with the numbers highlighted. These values refer to the ground-truth available in the databases (\*Ground-truth).

(degree)	Bunny	Dragon	Happy Buddha	Hammer
GT*	<b>45.000</b>	<b>24.000</b>	<b>24.000</b>	<b>45.000</b>
<i>ICP<sub>p2p</sub></i>	41.300	23.862	21.679	45.577
4PCS	42.582	24.423	23.744	44.673
SAC IA	39.992	23.491	20.626	44.691
Go-ICP	34.480	61.281	15.612	36.198
CP-ICP	16.498	<b>24.009</b>	22.543	44.590
Our	<b>43.245</b>	<b>24.009</b>	<b>24.039</b>	<b>45.042</b>

#### 4.3 Pairwise Registration of Outdoor Scenes

This is an experiment in which the challenges of outdoor scene perception are posed to the registration al-

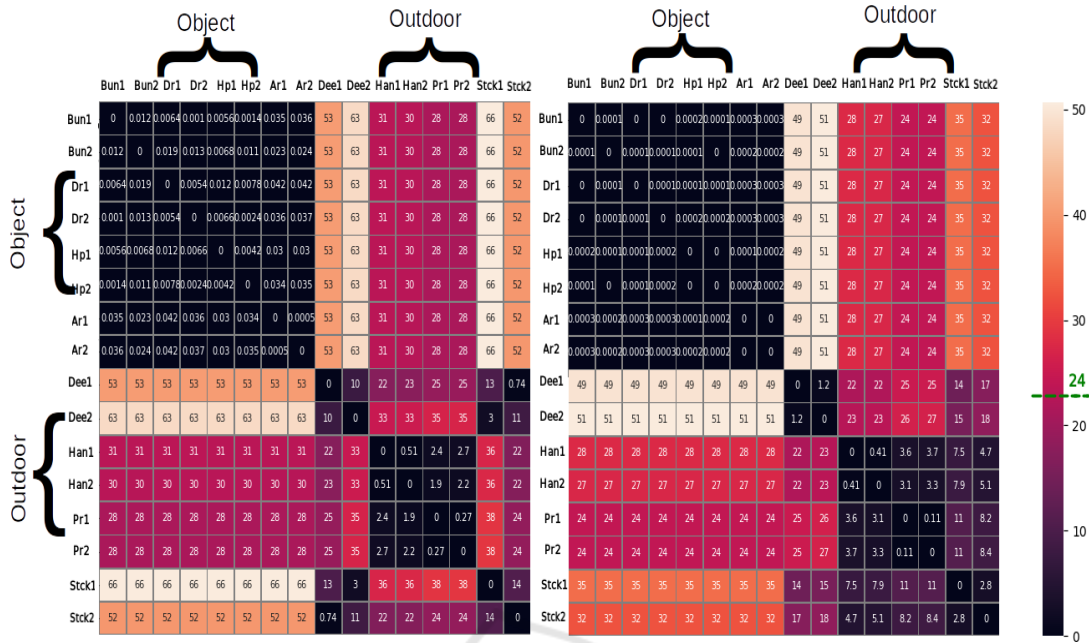


Figure 4: Heatmap-like images of Eigentropy and Omnivariance corresponding to Euclidean distances between pairs of the investigated samples. The darker areas correspond to close samples in the given space. The line in the color bar refers to the separation threshold between the classes.

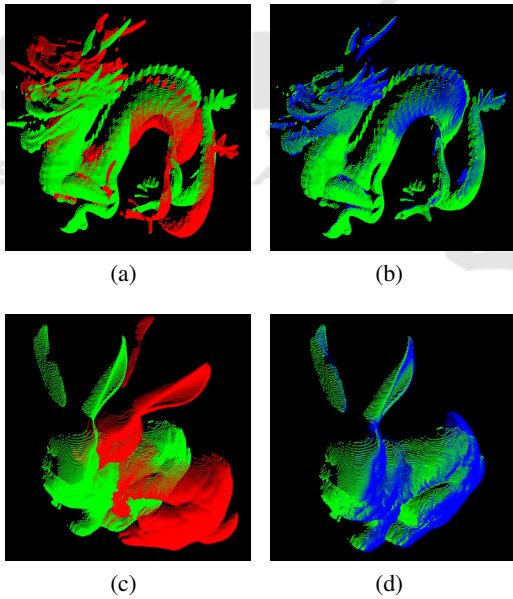


Figure 5: Result of alignment of Dragon and Bunny models. In (a) we have the initial dragon pose, in (b) the registration, in (c) the initial Bunny pose and finally, in (d) the registration of the Bunny model.

gorithm. Indeed, the surfaces to be matched are no more rigid ones and, therefore, the use of a rigid transformation approach for pose correction may simply fail. If the reader is less aware of the concept, think of the existence of moving people or cars and also of

Table 4: Time in seconds to correct the pose of pairs of objects.

(in sec.)	Bunny	Dragon	Happy Buddha	Hammer
<i>ICP<sub>p2p</sub></i>	9.427	7.527	17.084	0.356
4PCS	7.425	0.646	51.388	187.40
SAC IA	342.34	276.90	245.93	21.999
Go-ICP	36.537	35.847	36.288	36.198
CP-ICP	5.916	3.503	9.297	<b>0.157</b>
Our	<b>4.043</b>	<b>3.301</b>	<b>3.015</b>	0.294

trees with moving leaves in the different acquisition shots of the scenario; they all represent disturbance to the surface representation which could require local transformation matrices (or other nonrigid approach) for proper pose correction.

Results are brought in Tables 5 and 6, which report once again the root-mean square error between source and target models after registration and the elapsed time in the task. Compared to the other techniques, it is remarkable the impressive time-efficiency achieved by the proposed algorithm. The goodness of matching as measured by the RMSE metric showed to be good enough for many of purposes concerning scene 3D perception, as it can be illustrated in Figures 6(a) to 6(d), for example.

Table 5: RMSE obtained from registration between pairs of outdoor scenes.

	Hannover	Gasebo	Camp	Depart.
$ICP_{p2pl}$	0.406	0.309	15.597	3.047
GICP	0.451	0.429	32.655	4.582
NDT	0.408	0.324	<b>12.714</b>	8.084
$CP_{GICP}$	<b>0.336</b>	<b>0.201</b>	13.097	<b>2.708</b>
Our	<b>0.341</b>	<b>0.222</b>	<b>12.484</b>	3.631

Table 6: Time in seconds to correct the pose of pairs of outdoor scenes.

(in sec.)	Hannover	Gasebo	Camp	Depart.
$ICP_{p2pl}$	4.141	13.014	198.00	92.291
GICP	6.479	27.994	288.64	318.21
NDT	5.752	36.111	197.37	87.797
$CP_{GICP}$	6.939	117.69	265.25	1968.06
Our	<b>0.648</b>	<b>11.582</b>	<b>86.642</b>	<b>29.345</b>

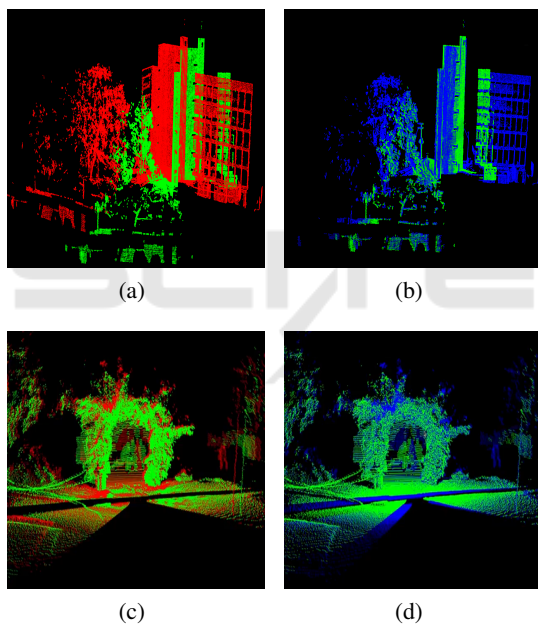


Figure 6: Result of the Department and Gasebo models alignment, respectively. In (a) we have the initial pose and in (b) the alignment for the Department model, in (c) the initial pose and in (d) the register for the Gasebo model.

## 5 CONCLUSIONS AND FUTURE WORK

In the present paper, it was introduced a registration algorithm for point-clouds originating from two different contexts, namely objects and outdoor environment. A look at the geometric descriptors based on the covariance matrix eigenvalues revealed that eigentropy and omnivariance can be used as features

and are able to simply and successfully separate the data samples corresponding to the mentioned contexts, whilst preserving the intraclass similarity for the whole and wide dataset prepared for the present investigation.

As future work, there is an improvement to pursuit regarding the possibility to switch among several registration cores, thus opening up the way to a many-context aware registration approach. Although this is strictly dependent on the availability of *ad-hoc* knowledge about the correspondence between a given technique and the context itself, which in turn relies on huge efforts of bibliographic reports surveying, it does pave the way towards fully-automatic registration methods to be embedded in robots or autonomous vision systems. Such an automatic system would obviously rely on very good stop criterion, which suggests a second relevant issue to deal with later: the search for alternatives to RMSE as registration quality measurement, since it often gives false or unacceptable quantitative representation of the goodness of matching.

## ACKNOWLEDGEMENTS

This work was financed in part by Fundação Cearense de Apoio ao Desenvolvimento Científico e Tecnológico (FUNCAP). This study was financed in part by the Coordenação de Aperfeiçoamento de Pessoal de Nível Superior - Brasil (CAPES) - Finance Code 001. The authors thank colleagues from the research group for the valuable comments. Authors also thank Marcus Forte and Fabricio Gonzales for acquiring and providing priority datasets.

## REFERENCES

- Aiger, D., Mitra, N. J., and Cohen-Or, D. (2008). 4-points congruent sets for robust pairwise surface registration. In *ACM Transactions on Graphics (TOG)*, volume 27, page 85. ACM.
- Aleotti, J., Rizzini, D. L., and Caselli, S. (2014). Perception and grasping of object parts from active robot exploration. *Journal of Intelligent & Robotic Systems*, 76(3-4):401–425.
- Besl, P. J. and McKay, N. D. (1992). Method for registration of 3-d shapes. *IEEE Transactions on Pattern Analysis and Machine Intelligence*.
- Chebroly, N., Läbe, T., and Stachniss, C. (2018). Robust long-term registration of uav images of crop fields for precision agriculture. *IEEE Robotics and Automation Letters*, 3(4):3097–3104.

- Chen, Y. and Medioni, G. (1992). Object modelling by registration of multiple range images. *Image and vision computing*, 10(3):145–155.
- Demantké, J., Mallet, C., David, N., and Vallet, B. (2011). Dimensionality based scale selection in 3d lidar point clouds. In *Laserscanning*.
- Donoso, F., Austin, K. J., and McAree, P. R. (2017). Three new iterative closest point variant-methods that improve scan matching for surface mining terrain. *Robotics and Autonomous Systems*, 95:117–128.
- Forte, M. D. N., Neto, P. S., The, G. A. P., and Nogueira, F. G. (2021). Altitude Correction of an UAV Assisted by Point Cloud Registration of LiDAR Scans. In *Informatics in Control, Automation and Robotics: 18th International Conference, ICINCO 2021 Online streaming, July 6-8, 2021*, volume 1.
- Hackel, T., Wegner, J. D., and Schindler, K. (2016). Fast semantic segmentation of 3d point clouds with strongly varying density. *ISPRS Annals of Photogrammetry, Remote Sensing & Spatial Information Sciences*, 3(3).
- Kurobe, A., Sekikawa, Y., Ishikawa, K., and Saito, H. (2020). Corsnet: 3d point cloud registration by deep neural network. *IEEE Robotics and Automation Letters*, 5(3):3960–3966.
- Levinson, J., Askeland, J., Becker, J., Dolson, J., Held, D., Kammel, S., Kolter, J. Z., Langer, D., Pink, O., Pratt, V., et al. (2011). Towards fully autonomous driving: Systems and algorithms. In *2011 IEEE intelligent vehicles symposium (IV)*, pages 163–168. IEEE.
- Levoy, M., Gerth, J., Curless, B., and Pull, K. (2005). The stanford 3d scanning repository.
- Liu, L., Shi, T., Liu, B., and Yao, H. (2020). Comparison of initial registration algorithms suitable for icp algorithm. In *2020 International Conference on Computer Network, Electronic and Automation (ICCNEA)*, pages 106–110. IEEE.
- Magnusson, M., Lilienthal, A., and Duckett, T. (2007). Scan registration for autonomous mining vehicles using 3d-ndt. *Journal of Field Robotics*, 24(10):803–827.
- Oliveira, F. P. and Tavares, J. M. R. (2014). Medical image registration: a review. *Computer methods in biomechanics and biomedical engineering*, 17(2):73–93.
- Rusu, R. B. and Cousins, S. (2011). 3d is here: Point cloud library (pcl). In *Robotics and automation (ICRA), 2011 IEEE International Conference on*, pages 1–4. IEEE.
- Segal, A., Haehnel, D., and Thrun, S. (2009). Generalized-icp. In *Robotics: science and systems*, volume 2, page 435.
- Siqueira, R. S., Alexandre, G. R., Soares, J. M., and The, G. A. P. (2018). Triaxial Slicing for 3-D Face Recognition From Adapted Rotational Invariants Spatial Moments and Minimal Keypoints Dependence. *IEEE Robotics and Automation Letters*, 3(4):3513–3520.
- Souza Neto, P., Pereira, N. S., and Thé, G. A. P. (2018). Improved Cloud Partitioning Sampling for Iterative Closest Point: Qualitative and Quantitative Comparison Study. In *15th International Conference on Informatics in Control, Automation and Robotics*.
- Vitter, J. S. (1984). Faster methods for random sampling. *Communications of the ACM*, 27(7):703–718.
- Wulf, O. (2016). Robotic 3d scan repository.
- Yang, J., Li, H., Campbell, D., and Jia, Y. (2016). Go-ICP: A Globally Optimal Solution to 3D ICP Point-Set Registration. *IEEE Transactions on Pattern Analysis and Machine Intelligence*.
- Zhang, Z. (1994). Iterative point matching for registration of free-form curves and surfaces. *International journal of computer vision*, 13(2):119–152.